Memory Subspaces for Temporal Locations Across Timescales in the Monkey Precuneus

Zhiyong Jin[1,4], Ning Su[1,2], Aakash Sarkar[3], Jiayu Cheng[1,5], Xufeng Zhou[1,2], Xuanlong Zhu[1], Makoto Kusunoki[6], Sze Chai Kwok[1,2,4,5] *

[1] Duke Kunshan University, Kunshan, China
[2] East China Normal University, Shanghai, China
[3] University of California San Francisco, San Francisco, USA
[4] Westlake University, Hangzhou, China
[5] Wuhan University, Wuhan, China
[6] University of Oxford, Oxford, United Kingdom

*sze-chai.kwok@st-hughs.oxon.org

Introduction

How the brain organizes the temporal structure of experience across different timescales remains unclear (Clayton & Dickinson, 1998). Here, we examine population dynamics in primate medial posterior parietal cortex during temporal order judgments (Zuo et al., 2026) spanning seconds to minutes and across-day episodes. We propose that temporal memory is supported by a unified low-dimensional manifold whose geometric integrity and dynamical structure enable accurate retrieval.

Task Paradigm and Results

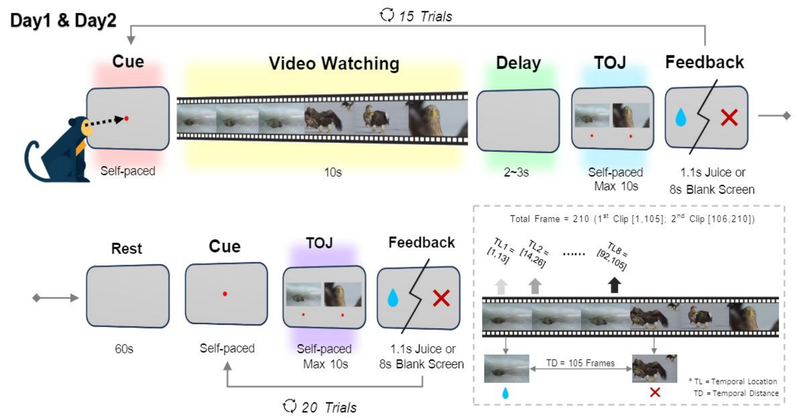

Fig. 1 TOJ memory task, three-day paradigm structure, and recording site. On Days 1 and 2, monkeys viewed 10-s videos (two concatenated 5-s clips). Following a 2-s delay, they performed a two-alternative forced-choice (2AFC) temporal order judgment (TOJ) on two extracted frames, identifying the earlier frame (15 trials). A 1-min retention interval preceded 20 additional TOJ trials without videoplay. Each day comprised four blocks with unique, unseen videos (8 clips each day). In addition, on Day 3, monkeys completed 120 TOJ trials integrating the full 16-clip set learned from preceding two days (*Bottom, Left*). Recording chamber and sites (*Botton, Right*).

Single-Neuron Temporal Location Selectivity

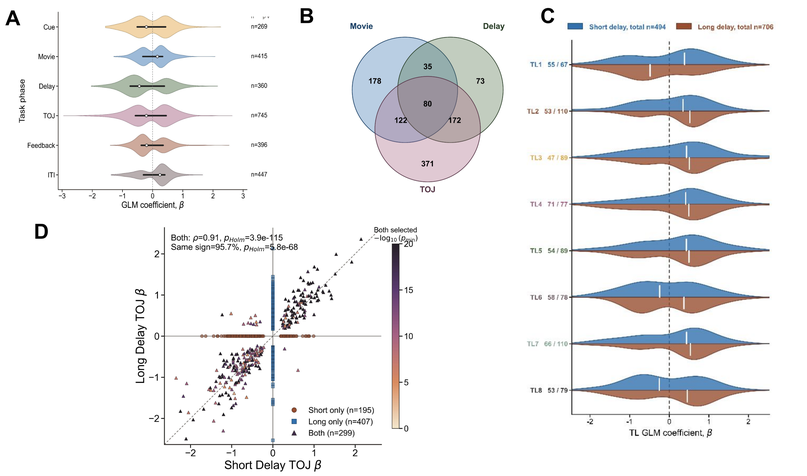

Fig. 2 Temporal location (TL) coding is distributed across task phases and remains stable across delay conditions. We fitted phase- and TL-level GLMs, quantified selectivity overlap among Movie, Delay, and TOJ, and compared TOJ modulation across delay conditions. (A) Significant modulation was observed throughout the task, with TOJ recruiting the largest neuronal population (n=745). (B) Phase selectivity showed substantial overlap: 409 neurons were selective in multiple phases, including 80 shared by Movie, Delay, and TOJ. (C) Long-delay TOJ recruited more neurons than short-delay TOJ (706 vs. 494). Among the 299 neurons selected in both conditions, β values were strongly correlated (ρ=0.91, p_Holm=3.9×10^{-115}), with 95.7% retaining the same modulation sign. (D) TL coding was detected across all eight temporal locations. Long-delay selections outnumbered short-delay selections at every TL, with the largest difference at TL2 (110 vs. 53). Most TLs showed positive modulation, whereas TL1, TL6, and TL8 changed polarity across delay conditions.

Dynamics of the Stimulus Subspace

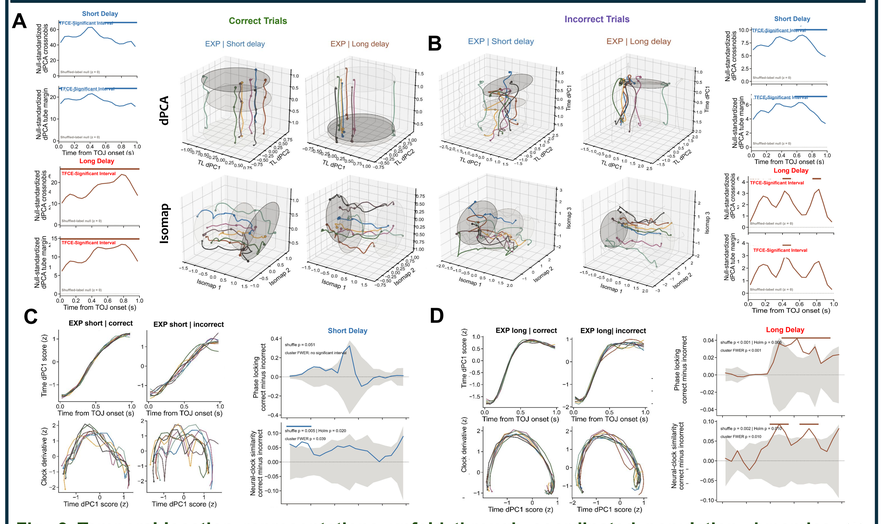

Fig. 3 Temporal-location representations unfold through coordinated population dynamics. (A) Correct-trial population activity formed distinct TL trajectories in dPCA and Isomap spaces under short- and long-delay conditions. dPCA crossnobis distance and tube margin were tested against 1,000 block-restricted TL-label permutations; horizontal bars mark TFCE-significant intervals. (B) Incorrect trials were analyzed using the same procedure. TL separation remained detectable, although the long-delay effect was smaller and limited to shorter intervals. (C) Under the short-delay condition, correct and incorrect trials followed different neural-clock dynamics. Neural-clock similarity was higher for correct trials, whereas the phase-locking difference almost reached significance. (D) Under the long-delay condition, correct trials showed higher phase locking and neural-clock similarity than incorrect trials. Thus, TL trajectories were present in both correct and incorrect trials, but their temporal coordination differed with retrieval outcome.

Population Coding of Temporal Location

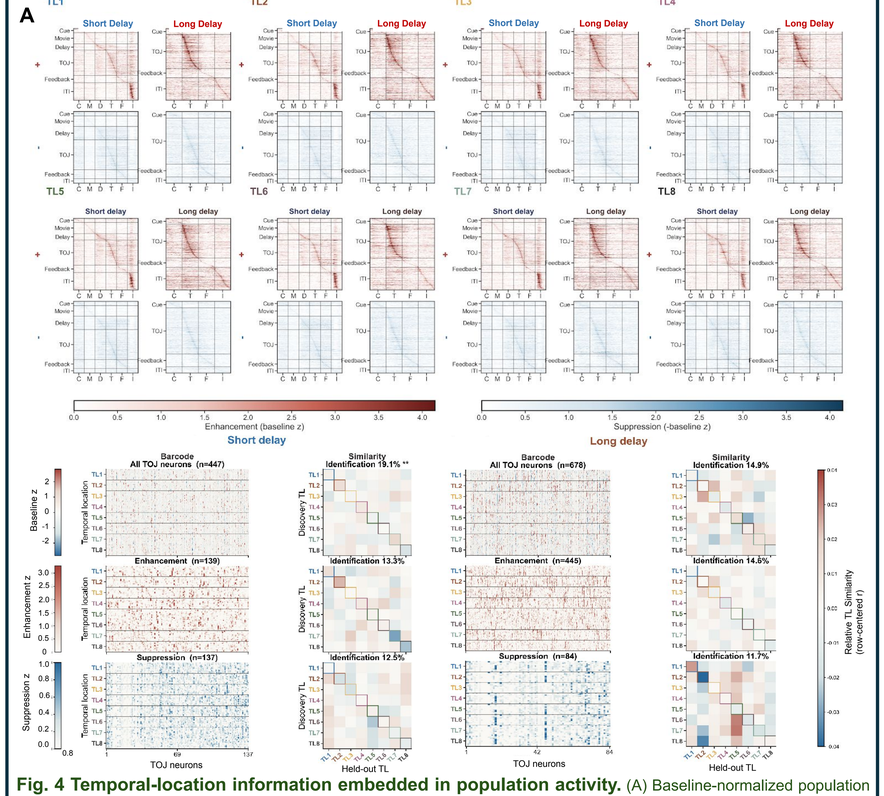

Fig. 4 Temporal-location information embedded in population activity. (A) Baseline-normalized population PSTHs grouped by TL1–TL8 and separated into enhancement and suppression. Both short- and long-delay trials showed temporally ordered activity patterns. (B) Population barcodes summarized neuron-wise response profiles, while discovery-versus-held-out similarity matrices assessed the stability of TL-specific patterns. The full short-delay population showed the strongest TL identification (19.1%, **; n=447), whereas its enhancement and suppression subsets were near chance (13.3% and 12.5%). Long-delay identification reached 14.9% for all neurons (n=678), 14.6% and 11.7% for enhancement and suppression, respectively. These results suggest that TL identity is best preserved by the combined population response.

Population Activity and Pair-Anchor Analysis Framework

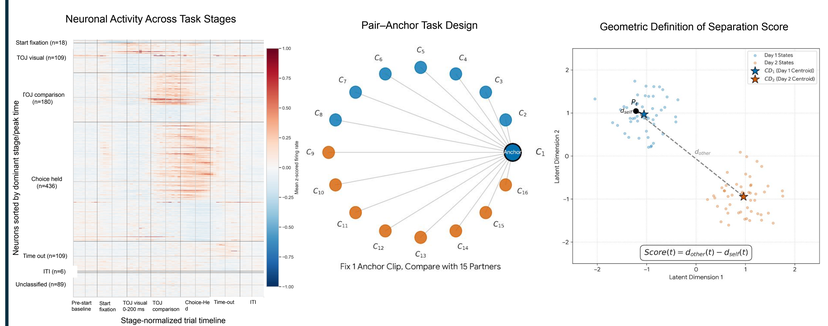

Fig. 5 Population activity and pair-anchor framework for quantifying day-specific separation. Stage-normalized population PSTH for Day 3 data (n=947), grouped by dominant stage and sorted by firing peak time (*Left*). Pair-Anchor Task Design. Schematic of analysis framework where neural trajectories are compared by fixing one clip as an Anchor and pairing it with 15 other Partner clips from Day 1 and Day 2 (*Middle*). Neural population activity was organized as a neurons × conditions × time tensor and projected into a dPCA subspace fitted within a cutoff window (-0.5 s to the shortest meanRT). Population activity was projected into a task-aligned dPCA subspace. For each point in each day-specific cluster, we compared their distance to the centroid of the other cluster (d_{other}) vs. to its own cluster (d_{own}) as a function of time (d_{other} (t) − d_{own} (t)) (*Right*).

Day-Specific Representational Geometry During Temporal Order Judgment

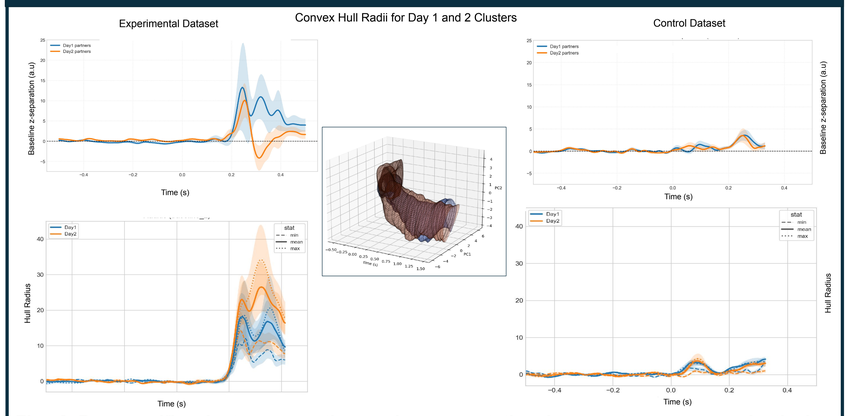

Fig. 6 Day-specific cluster separation and representational geometry emerge selectively during temporal order judgment on Day 3. A separation (computed as d_{other} (t) − d_{own} (t), see Fig. 5) between the day clusters is seen after onset of TOJ for the main experiment (*Top Left*), but not in control experiment (*Top Right*, n=450). Convex hulls enclosing day-specific clusters show that the more recent Day-2 cluster shows a clearly larger emergent radius, which corresponds to a higher representation volume of its hull (*middle*) compared to Day-1, but only for the experimental dataset (*Bottom Left*), while such separation dynamics are not seen in the control dataset (*Bottom Right*). Hull radius was defined as centroid-to-boundary distance.

Conclusion

- The macaque precuneal neurons represent temporal locations through a unified computational framework. The shared modulation across scales suggests a stable neuronal axis for temporal indexing (Sarkar et al., 2026).
- The "manifold collapse" in error trials reveals the geometric basis of behavioral failure. The combination of neural clock and phase portrait dynamics suggests that retrieval context shapes episodic representations at multiple geometric levels.
- Memories of Day 1 and Day 2 events differ not only in where their trajectories are centered, but also in how their manifolds expand over time. Null effects in the control dataset suggest that these geometric differences reflect meaningful episodic organization.

References and Acknowledgments

- Clayton, N. S., & Dickinson, A. (1998). Episodic-like memory during cache recovery by scrub jays. *Nature*, *395*(6699), 272-274.
- Zuo, S., Wang, C., Wang, L., Jin, Z., Zhou, X., Su, N., ... & Kwok, S. C. (2026). Neural population dynamics and temporal context cells in macaque medial parietal cortex support temporal order memory. *PLoS biology*, *24*(4), e3003759.
- Sarkar, A., Wang, C., Zuo, S., & Howard, M. W. (2024). "What" x "When" working memory representations using Laplace Neural Manifolds. *arXiv preprint arXiv:2409.20484*

The work received support from the Kunshan Municipal Government research funding grant (24KKSGR017) and Duke University Provost Fund for Duke–DKU Collaborations (25KINTL013) (SCK).